P.Y. Zheng, T. Zhou, and D. Gall, Semiconductor Sci. Technol. **31**, 055005 (2016).

Electron channeling in TiO_2 coated Cu layers

*Pengyuan Zheng, Tianji Zhou and Daniel Gall**
Department of Materials Science, Rensselaer Polytechnic Institute, Troy,NY 12180, USA
E-mail: galld@rpi.edu

Abstract

Electron transport in metal conductors with ~5-30 nm width is dominated by surface scattering. *In situ* transport measurements as a function of surface chemistry demonstrate that the primary parameter determining the surface scattering specularity is the localized surface density of states at the Fermi level $N(E_f)$. In particular, the measured sheet resistance of epitaxial Cu(001) layers with thickness d_{Cu} = 9-25 nm increases when coated with d_{Ti} = 0.1-4.0 monolayers (ML) of Ti, but decreases again during exposure to 37 Pa of O_2. These resistivity changes are a function of d_{Cu} and d_{Ti} and are due to a transition from partially specular electron scattering at the Cu surface to completely diffuse scattering at the Cu-Ti interface, and the recovery of surface specularity as the Ti is oxidized. X-ray reflectivity and photoelectron spectroscopy indicate the formation of a 0.47±0.03 nm thick Cu_2O surface layer on top of the TiO_2-Cu_2O during air exposure, while density functional calculations of TiO_x cap layers as a function of x = 0-2 and d_{Ti} = 0.25-1.0 ML show a reduction of $N(E_f)$ by up to a factor of four. This reduction is proposed to be the key cause for the recovery of surface specularity and results in electron confinement and channeling in the Cu layer upon Ti oxidation. Transport measurements at 293 and 77 K confirm the channeling and demonstrate the potential for high-conductivity metal nanowires by quantifying the surface specularity parameter p = 0.67±0.05, 0.00±0.05, and 0.35±0.05 at the Cu-vacuum, Cu-Ti, and Cu-TiO_2 interfaces.

Key words: Electron surface scattering, resistivity size effect, electron channeling, copper interconnect, TiO_2-Cu interface.

1. Introduction

Electron transport at reduced length scales is attracting continuous interest due to its broad impact on nanoelectronics and on the understanding of materials properties [1-6]. The size effect in metal layers and wires refers to the increase in the electrical resistivity as the cross-sectional length scale approaches or becomes smaller than the bulk mean free path for electron-phonon scattering [7-12]. The increase associated with electron surface scattering is most commonly described within the framework of Fuchs [13] and Sondheimer [14] (FS), which uses a phenomenological scattering parameter p to describe scattering events as either specular ($p = 1$) or diffuse ($p = 0$). Specular scattering causes no resistivity increase and is required to achieve high-conductivity nanowires that will facilitate the viable development of advanced integrated circuits [9-11,15,16], flexible transparent conductors [17-19], thermoelectric power generation [20,21], magnetic sensors [8] and spintronics [22]. However, a basic understanding of what surface chemistry and structure parameters determine the specularity p is still lacking. Recent research on electron scattering at Cu surfaces suggests that it is strongly affected by the adjacent layer material and/or the interface structure. More specifically, atomically flat single crystal Cu(001) surfaces exhibit partially specular electron scattering with $p = 0.6$ if held in vacuum [23], but the scattering becomes completely diffuse ($p = 0$) after exposure to oxygen [24] or air [25-28], which is attributed to surface oxide formation which causes an irregular disturbance of the electron potential at the surface.[29] Electron scattering at the interface between Cu and barrier metals including Ta [4,11,12], Zr [31], Hf [31], and TiN [32] has also been reported to yield completely diffuse scattering or to cause resistivities that are even higher than what is expected for $p = 0$. In contrast, there are a few reports that suggest partial specular scattering at the interface between Cu and an add-layer, including scattering at the epitaxial Cu(001)/Ni(001) interface with $p = 0.3$ [27], Cu/SiO_2 interface with $p = 0.33$ [33] and a time dependent resistivity decrease for Ta and Al coated Cu which indicates increasing specularity due to oxidation of the coating [34]. The latter result may be attributed to the so called “electron channeling effect ”[35], which has been used to explain the strong specular reflection reported for the Au/Fe interface[36] and the specular scattering predicted at magnetic multilayer interfaces in giant magnetoresistance (GMR) applications [37,38], where spin-dependent scattering is responsible for spin dependent confinement of electrons in the nonmagnetic layer of GMR structures [39]. More generally, electron channeling occurs if the interface or multi-layer electronic structure

confines electrons within the high conductivity layer, which is achieved through (a) a reduction of the localized density of states (LDOS) at the interface [40], (b) a mismatch of the Fermi momentum component parallel to the interface in adjacent layers [35], or (c) a large potential step at the interface [41,42]. The motivation for the present work is the promise that electron channeling effects may be exploited to suppress electron scattering from metallic conductors into adjacent layers which yields, for example, high-conductivity Cu lines with specular interface scattering for integrated nanoelectronics.

Electron scattering at the Cu-Ti interface is still relatively unexplored despite that Ti layers have recently been demonstrated as self-forming diffusion barriers for Cu interconnects [44]. Ti additions have been reported to increase the Cu resistivity, which has been attributed by some researchers to smaller grains and a larger grain boundary reflection coefficient due to Ti segregation to the grain boundaries [45], while others attribute it to completely diffuse scattering at the Cu-Ti interface [46]. In order to deconvolute the surface scattering effect from the grain boundary scattering [47,48] and to determine the electron scattering specularity at the Cu-Ti interface, we use in the present investigation samples without grain boundaries, that is epitaxial Cu(001) layers with good crystalline quality and smooth surfaces [49,50]. Furthermore, we demonstrate the possibility of electron channeling by studying the electron scattering while oxidizing the Ti layer, which effectively reduces the LDOS at the interface. In particular, we show in this report that electron scattering at the Cu-Ti interface is completely diffuse, as determined from thickness dependent resistivity measurements on Ti-coated epitaxial Cu(001) at both 293 and 77 K, and provide direct experimental evidence for partially specular scattering with p = 0.35±0.05 at the TiO_2-Cu interface. *In situ* O_2 exposure of Ti-coated Cu causes a gradual decrease in the resistance which is attributed to reduction in the LDOS associated with Ti oxidation, as confirmed by the calculated electronic structure of Cu(001) coated with TiO_x as a function of x = 0-2.

2. Experimental and Computational Approach

Epitaxial 9-25 nm thick Cu(001) layers are grown on MgO(001) substrates in 3.5 mTorr 99.999% pure Ar at T_s = 60 °C in a multi-chamber sputter deposition system with a base pressure <10^{-9} torr, as described in Ref. [27]. After deposition, the layers are transported without breaking vacuum to an adjacent analysis chamber maintained at a base pressure of 10^{-9} Torr for

in situ room temperature sheet resistance measurements using a spring loaded linear four point probe operated at 1-100 mA [23]. The samples are allowed to self-cool to room temperature and thermal equilibrium is considered to be reached when the measured voltage approaches a constant value that varies less than 0.1% per 1 h. Subsequently, some samples are transferred back for growth of a Ti cap layer with a nominal thickness of 0.016-0.62 nm (0.1-4.0 monolayers), deposited at 0.003 nm/s and T_s = 40 °C, followed by additional *in situ* resistivity measurements. The layer resistivity is determined from the measured sheet resistance and the Cu thickness obtained from X-ray reflectivity measurements described below. We note here, that the additional transport through the Ti coating is neglected when determining the resistivity values, since a simple parallel conductor model suggests the Ti to cause a maximum 0.4% correction in ρ based on the measured ρ of a 14.8 nm thick Ti film, but the actual correction is expected to be much smaller than 0.4% due to the size effect in the 0.62 nm Ti cap layer. The change in resistance of Cu and Ti/Cu layers as a function of oxidation time t_{ox} is studied by injecting a 90% Ar – 10% O_2 mixture at a constant flow rate into the analysis chamber to reach a steady state pressure of 370 Pa while continuously measuring the resistance. The delay between the time when the valve of the gas inlet is opened until the gas mixture reaches the sample surface is corrected for by setting the oxidation starting time t_{ox} = 0.1 s as the time when the onset of the sheet resistance change is greater than the standard deviation of the measurement, which is 0.2-0.4%.

All samples are removed from the vacuum through a load lock filled with N_2 gas and dropped quickly (less than 2 s) into liquid N_2 to minimize air-exposure. The resistivity is measured again, first at 77 K submersed in N_2 and then at room temperature (RT) of 293±1 K after warm up using a continuous flux of dry commercial grade N_2 gas. The samples are subsequently stored inside a desiccator kept at < 5% humidity and removed for additional RT and 77 K resistivity measurements after different time intervals to evaluate the effect of air exposure time. The thickness and roughness of each film is determined, within < 30 minutes after exposing the sample to atmospheric air, by x-ray reflectivity (XRR) using a PANalytical X'pert PRO MPD system with a Cu K_α source, a parabolic mirror yielding a parallel beam with a 0.029° divergence, and a 0.27° acceptance parallel plate collimator in front of a scintillator point detector. The epitaxy is confirmed by x-ray diffraction (XRD) ω-2θ scans, ω-rocking curves, and ϕ scans of Cu 111 reflections, similar to the procedure described in Refs. [80,81] and [53] for

epitaxial ScN(001), $Sc_{1-x}Al_xN$(001) and W(001) layers. The XRD results show that all layers are Cu(001) single crystals with a negligible strain of 0.03-0.25%. X-ray photoelectron spectroscopy (XPS) is carried out using a PHI 5000 Versaprobe™ with an Al K_α source (1486.6 eV). Photoelectrons are collected at an angle θ = 5°, 15°, 45°, 55° and 90° relative to the sample surface, using an energy step size of 0.05 eV and a detector pass energy of 23.5 eV for the Ti2p photoelectrons and of 11.75 eV for the Cu2p, O1s and C1s electrons.

First-principles electronic structure calculations of Cu thin films with Ti or Ti oxide cap layers are done using the Vienna *Ab initio* Simulation Package (VASP), employing the projector-augmented wave (PAW) method [82,83], the Perdew-Burke-Ernzerhof (PBE) exchange correlation functional [56], periodic boundary conditions, and a plane-wave basis set with a cut-off energy of 300 eV, and pseudopotential that include all core electrons up to the Cu 3*p*, Ti 3*p*, and O 1*s* electrons. All simulations are done with a $\sqrt{2}a \times \sqrt{2}a \times 15a$ supercell, where a = 0.3615 nm is the bulk fcc lattice constant of Cu which is kept constant throughout the calculations. The Cu(001) surface is simulated using 24 Cu atoms that form a 1.1 nm thick Cu film consisting of 6 monolayers (ML) adjacent to a 4.3 nm thick vacuum layer. This Cu thickness is considered sufficient as it yields comparable electronic properties including Fermi velocity and ballistic conductance as is obtained from calculations of bulk Cu. In addition, the position of the Fermi level in the middle of the 6 Cu MLs is found to be unaffected by the surface structure including the Ti and O adatoms, as confirmed by the calculated energy difference between the Fermi level and the first peak of the Cu 3*d* valence band at the center of the simulated Cu(001) layer, which remains 1.6±0.1 eV for all calculations. A Ti cap layer is simulated using 1-4 Ti adatoms on the Cu(001) surface, corresponding to a 0.25-1.0 ML surface coverage, while the oxidized Ti cap is obtained using both Ti and O adatoms with the O-to-Ti ratio x ranging from 0.25 to 2. All simulations assume a growth mode where Ti wets and covers the Cu surface, similar to the reported nearly layer-by-layer growth of Co on Cu [57,58] and cubic Ti on MgO [59]. The most stable configuration for a given number of Ti and O adatoms is searched for by relaxing a set of 2-8 different initial configurations for each simulated coverage, using a conjugate-gradient algorithm [60] to relax all adatoms as well as the four Cu atoms in the top copper layer, while the remaining Cu atoms are kept fixed at their bulk positions. The relaxed atomic positions of the various structures are listed in the supporting information SI.2. The electronic structure is obtained for the relaxed structures using a self-consistent calculation with a 30×30×1 *k*-point

grid. Subsequently, a non-self-consistent calculation with the same *k*-point grid is conducted in order to determine the density of states at the surface by projecting the wave functions of each band onto local atomic orbitals around each ion for the surface layers with a quick projection scheme within the PAW method. [82,83] The local density of states (LDOS) at the surface is determined for 300 energy points within 20 eV below to 10 eV above the Fermi level. The number of bands in the self-consistent calculations is set such that there are 36-68 empty bands, yielding a converged DOS for all energies ≤ 2.7 eV above the Fermi level for all calculations.

3. Results and Discussion

Figure 1 is a plot of the measured sheet resistance R_s of four Cu(001) layers that are capped with Ti overlayers and subsequently exposed to oxygen with a partial pressure P_{O2} = 37 Pa. All layers have the same Cu thickness d_{Cu} = 9.5±0.1 nm but different nominal thicknesses of the Ti cap layer d_{Ti} = 0-0.62 nm, corresponding to 0, 0.1, 1.0, and 4.0 ML, where d_{Ti} = 0 ML refers to a sample without cap layer. The data points on the left in Figure 1 are the sheet resistances of the pristine Cu layers without Ti cap. These nominally identical samples have comparable measured values for R_s of 3.94±0.04, 3.68±0.06, 3.85±0.04, and 3.80±0.04 Ω/sq, indicating the good experimental reproducibility of the Cu deposition and of the *in situ* resistivity measurements. The next set of data points show the measured resistance after the deposition of a 0.1, 1.0, and 4.0 ML thick Ti cap layer, which causes an increase in R_s of 0.15, 1.22 and 1.65 Ω/sq, respectively. This increase is attributed to increasingly diffuse surface scattering caused primarily by localized surface states and atomic-level roughening associated with the added Ti, resulting in completely diffuse scattering for d_{Ti} = 1.0 ML as discussed in detail below. The increase in R_s is even slightly larger for d_{Ti} = 4.0 ML than d_{Ti} = 1.0 ML, which is the result of a reduced Cu conducting thickness as some Cu is consumed in a Ti-Cu surface alloy, as quantified by the XRR and XPS analyses presented below.

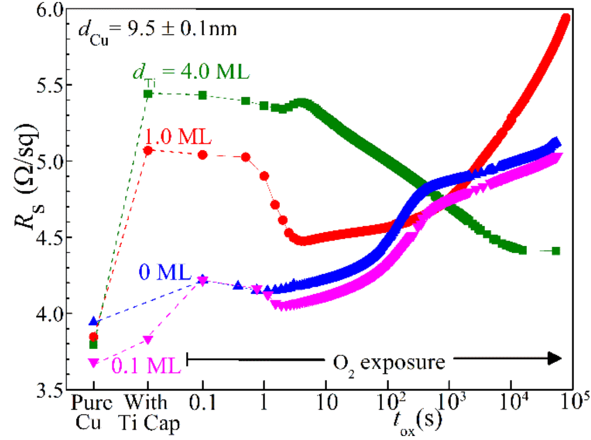

Figure 1. Sheet resistance R_s of four 9.5±0.1 nm thick epitaxial Cu(001) layers with pure Cu surfaces, coated with 0, 0.1, 1.0, or 4.0 ML of Ti, and vs exposure time t_{ox} to a 37 Pa O_2 partial pressure.

The subsequent data shows the measured R_s as a function of oxidation time t_{ox}. The sheet resistance of the pristine Cu layer (d_{Ti} = 0 ML) increases from 3.94 prior to oxygen exposure to 4.22 Ω/sq within ≤ 0.1 s and drops back to 4.15 Ω/sq for t_{ox} = 1.1 s. A similar increase and subsequent decrease has previously been reported and is attributed to the disturbance of the surface potential by physisorbed O_2 which causes diffuse electron scattering for a partially covered surface but specular scattering for a complete and smooth O_2 overlayer that results in a flat surface potential [24]. Further exposure to O_2 causes a continuous increase in R_s to reach 5.12 Ω/sq at t_{ox} = 54420 s when the experiment is terminated. This increase is attributed to increasingly diffuse surface scattering due to localized oxide surface states and the disturbance of the surface potential by oxidation of the copper surface, and ultimately the reduction of the metallic Cu thickness [27]. The change in slope in the logarithmic plot is attributed to different stages of copper surface oxidation including Cu_2O islands nucleation, surface saturation, and growth at a decreased rate [61]. The sample with d_{Ti} = 0.1 ML exhibits a similar R_s curve during oxygen exposure, agreeing both qualitatively and quantitatively with the curve from as the pristine Cu layer. This indicates that Ti adatoms with a 10% surface coverage have a negligible effect on Cu_2O nucleation or growth.

In contrast, the Cu layer covered with a 1.0 ML Ti cap shows a dramatically different resistance curve during oxygen exposure. R_s drops quickly from 5.07 Ω/sq to a minimum of 4.47 Ω/sq at t_{ox} = 4.5 s, followed by a continuous rise to 5.93 Ω/sq at t_{ox} = 78052 s. The initial decrease is attributed to oxidation of the Ti layer, as discussed in detail below. The subsequent

increase is due to Cu oxidation which leads to diffuse surface scattering. This increase is considerably steeper than for d_{Ti} = 0 and 0.1 ML. In particular, while the pristine Cu layer reaches a maximum R_s = 5.12 Ω/sq at the end of the experiment, the same resistance is reached an order of magnitude earlier, after 5511 s for d_{Ti} = 1.0 ML. This faster change to completely diffuse scattering is attributed to a larger Cu oxidation rate for d_{Ti} = 1.0 ML, associated with the presence of Ti^{4+} ions at the surface, which increase the Cu cation vacancy concentration and, in turn, facilitate Cu diffusion and continued oxidation of the Cu layer [62]. R_s for d_{Ti} = 1.0 ML continues to increase at a relatively high rate for t_{ox} > 5511 s, indicating a reduction of the Cu conducting cross-section due to Cu (bulk) oxidation which is also facilitated by the Ti^{4+} ad-ions.

The curve for d_{Ti} = 4.0 ML in Figure 1 shows an initial slight decrease by 0.14 Ω/sq to 5.3 Ω/sq at t_{ox} = 2.0 s, followed by an increase to 5.38 Ω/sq at t_{ox} = 4.0 s and a subsequent continuous decrease to 4.41 Ω/sq at t_{ox} = 15545 s after which R_s remains approximately constant until the end of the experiment at t_{ox} = 53728 s. The initial dip and small increase is, analogous to the explanation for the Cu-vacuum interface at the pristine Cu surface, attributed to a transition from diffuse to partial specular to diffuse scattering at the Ti-vacuum interface, associated with an increasing surface coverage of physisorbed and subsequently chemisorbed oxygen, which initially slightly reduces the LDOS at the Ti surface and then causes a perturbation of the flat surface potential at the Ti-vacuum interface. The subsequent drop occurs over more than three orders of magnitude of O_2 exposure time, from t_{ox} = 4.5 to 15545 s, and follows an approximately logarithmic decrease as indicated by the nearly straight curve in the log-scale plot. A logarithmic time dependence is expected for the kinetics of initial Ti oxidation [63], suggesting that the continuous decrease of R_s is directly associated with the gradual oxidation of the Ti layer. The fact that R_s reaches a plateau at t_{ox} > 15545 s suggests that the Ti is completely oxidized, while the Cu oxidation is sufficiently suppressed such that no increase in R_s can be detected within the experimental time. Comparing the rate of decrease of R_s with that of the d_{Ti} = 1.0 sample indicates that oxidation of 4 ML of Ti takes three to four orders of magnitude longer than for oxidation of 1 ML, which is attributed to the more stable passive 4 ML thick Ti. We also note that the global minima in R_s after O_2 exposure have comparable values for d_{Ti} = 1.0 and 4.0 ML, suggesting that this value is defined by the degree of specular scattering at the Cu-TiO_2 interface, while the thickness of the TiO_2 does not affect the electron scattering at the Cu-TiO_2 interface. Similar changes in R_s during Ti deposition and subsequent oxidation is also observable

for polycrystalline Cu layers, as described in the supporting information SI.1. In the following, we attribute the decrease in R_s during oxidation to the reduction of the density of surface states, resulting in the recovery of specular surface scattering.

Figure 2 (a) is a plot of the local density of states at the surface of a pristine 6-ML-thick Cu(001) layer, obtained by projecting the wave functions onto local orbitals centered around the surface atoms of the top monolayer. It is plotted over a selected energy range from -8 to 4 eV, where the Fermi level E_f is set to 0 eV. The main features in the DOS are associated with the Cu 3*d* bands, exhibiting 4 peaks at -1.6, -2.2, -2.9, and -4.0 eV and 2 shoulders at -3.3 and -4.5 eV, matching well the previously reported features from the surface layer in a 7-ML-thick Cu(001) layer [64]. The DOS at the Fermi level $N(E_f)$ is 3.7 $eV^{-1}nm^{-2}$, which is close to that of bulk Cu with a reported $N(E_f)$ = 3.6±0.1 $eV^{-1}nm^{-2}$ [65]. Figure 2(b) is the corresponding plot from the surface of a Cu(001) layer that is covered with a monolayer of Ti. It is the DOS from orbitals that are centered around the Ti surface atoms which occupy relaxed positions that are close to expected bulk lattice sites. That is, the Ti atoms approximately extend the Cu crystal by an additional monolayer. The Fermi level crosses the wide Ti 3*d* band which extends approximately from -2.0 to 4.5 eV. This results in a relatively large $N(E_f)$ = 27.4 $eV^{-1}nm^{-2}$. A smaller Ti coverage of 0.25 and 0.5 ML Ti yields lower $N(E_{\mathrm{f}})$ values of 15.0 and 22.1 $eV^{-1}nm^{-2}$, as also presented below. Figure 2(c) shows the surface density of states of an oxidized Ti monolayer on Cu(001). This structure contains four Ti and eight O atoms covering a 0.511×0.511 nm^2 surface area within the calculated supercell. That is, the number of Ti atoms correspond to a metallic monolayer which, however, during oxidation develops into a rutile-like four-layer TiO_2 structure. The in-plane lattice constant is kept fixed at the bulk Cu value, such that this simulated TiO_2 structure exhibits an 11% biaxial tensile strain relative to the reported bulk rutile TiO_2. The plotted DOS is from the local orbitals around both the Ti and O atoms and shows splitting of the hybridized O2*p*–Ti3*d* bands into an occupied valence band at -6.5 to -2.0 eV and an empty conduction band just above the Fermi level at 0.0-4.0 eV, with primarily O2*p* and Ti3*d* character, respectively. In addition, a tail of the Cu4*s* states from the underlying Cu layer contributes to the LDOS, as confirmed using test calculations without a Cu under layer. These Cu states result in a non-zero density at the Fermi level of $N(E_f)$ = 6.5 $eV^{-1}nm^{-2}$. This value may, however, be relatively sensitive to the exact strain state and atomic configuration, considering the large slope of the DOS at E_f. More specifically, the simulated band gap of 1.5±0.1 eV is considerably

smaller than the experimental gap for bulk TiO_2 of 3.3-4.0 eV [66], as well as 2.6 eV predicted for a thin film by DFT with an LDA functional [67], and 3.39 or 3.46 eV for bulk TiO_2 predicted using a hybrid HSE06 functional or a G_0W_0 method, respectively [66]. The relatively small gap may be attributed to the common underestimation of gaps in DFT-PBE, which yields a 1.88 eV gap for bulk TiO_2 [66], but may also be related to band broadening due to the strained structure, such that the calculated value for $N(E_f)$ is likely overestimating the DOS at the Fermi level of a relaxed TiO_2 layer on Cu(001). In addition, band tails from the Cu4*s* states also contribute to $N(E_f)$, as confirmed by test calculations of the strained TiO_2 without supporting Cu layers, yielding a smaller $N(E_f)$ and a TiO_2 band gap of 1.8±0.1 eV.

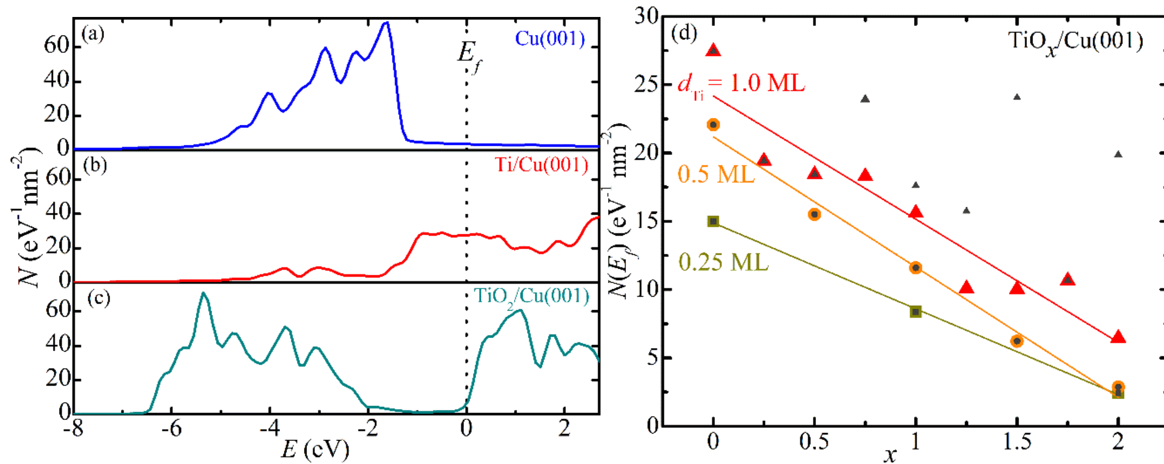

Figure 2. The projected density of states N per surface area of a 6 ML-thick Cu(001) layer for (a) a pristine Cu surface, (b) a surface with a 1.0 ML Ti cap, and (c) a TiO_2 surface layer, calculated using density functional calculations with a 4-atoms-per-ML supercell. (d) N at the Fermi level E_f for Ti coverages of 0.25, 0.5, and 1.0 ML as a function of O-to-Ti ratio x. The colored symbols indicate the relaxed configurations with the lowest $N(E_f)$ values while the smaller black symbols indicate the $N(E_f)$ of the lowest energy configuration within the constraints of the supercell.

The band splitting and the $N(E_f)$ is also a function of the Ti coverage and the degree of oxidation, as summarized in Figure 2(d) which is a plot of the calculated $N(E_f)$ for d_{Ti} = 0.25, 0.5, and 1.0 ML as a function of the O-to-Ti ratio x in TiO_x cap layers on Cu(001). The data points are obtained by projecting the calculated wave function onto local orbitals around Ti and O atoms, which are occupying relaxed positions on top of the Cu(001) layer. For d_{Ti} = 0.25 and 0.5 ML, atomic relaxation from most initial configurations with a given d_{Ti} and x converge to the same lowest energy structure. In contrast, d_{Ti} = 1.0 ML involves relaxation of 4 Ti and up to 8 O atoms which results in a thicker cap layer and multiple configurations in local energy minima

where the Ti atoms form an approximately flat single layer for $x = 0$-0.5, but are most stable in a bi-layer structure for $x = 0.75$-1.5 and 2.0, while separated into four layers forming a rutile-like structure for $x = 1.75$. Typically, the energetically most preferred TiO_x structure is the most fully oxidized with lowest DOS at E_f, but exceptions arise due to epitaxial unit cell constraints, leading to more metallic bonded structures. In particular, for $d_{Ti} = 1.0$ ML, the lowest energy configuration does not always coincide with the structure with the highest degree of oxidation (for a given x), which we attribute to the lateral constraint from the periodic boundary condition with a fixed period. To illustrate this, the plot in Figure 2(d) shows as small black symbols the calculated $N(E_f)$ for the lowest energy configurations for each d_{Ti} and x, and larger colored symbols for the structure with the lowest calculated $N(E_f)$. For $d_{Ti} = 0.25$ and 0.5 ML, black and colored data points coincide, while for $d_{Ti} = 1.0$ ML, they coincide for low oxygen concentrations $x \leq 0.5$ but deviate for $x \geq 0.75$ except for $x = 1.75$.

The calculated $N(E_f)$ plotted in Figure 2(d) decreases with increasing oxidation, from 15.0 $eV^{-1}nm^{-2}$ at $x = 0$ to 2.4 $eV^{-1}nm^{-2}$ at $x = 2$ for $d_{Ti} = 0.25$ ML, and similarly from 22.0-2.9 $eV^{-1}nm^{-2}$ and from 27.4-6.5 $eV^{-1}nm^{-2}$ for $d_{Ti} = 0.5$ and 1.0 ML, respectively. The decrease in $N(E_f)$ is approximately linear in x, as indicated by the straight lines through the data points which are obtained from a linear fit. This decrease in the LDOS at the surface is used as the primary argument to explain the decrease in R_s upon oxidation of Ti cap layers. More specifically, electrons that approach the Cu surface are reflected back into the conductor if the surface is smooth and the density of localized states at the surface is negligible, as is the case for pristine Cu(001) which leads to partially specular scattering [27]. However, a Ti cap layer, as shown in Figure 2(b), causes a large $N(E_f)$. Consequently, electrons are scattered into these states, loose their momentum and ultimately return into the conductor with a random direction, which effectively results in diffuse scattering and a correspondingly higher R_s for the Ti coated Cu in comparison to the pristine Cu, as shown in Figure 1. Subsequent oxidation of the Ti cap layer leads to a continuous reduction in $N(E_f)$ with increasing x in TiO_x, resulting in increasingly specular surface scattering and a reduction in R_s, as observed experimentally for $d_{Ti} = 1.0$ ML and $t_{ox} < 4.5$ s, and for $d_{Ti} = 4.0$ ML and $t_{ox} < 15545$ s.

Figure 3 shows the results from a detailed analysis of the surface layer chemistry and structure using a combination of angle resolved XPS and XRR in (a) and (b), respectively. The

data is from Cu(001) layers with thickness d_{Cu} = 9.90±0.05 and 14.70±0.05 nm that are coated with 4.0 ML of Ti and are exposed to air. The inset in Figure 3(a) shows typical XPS spectra obtained at a normal electron emission angle θ = 90°, showing the Cu $2p_{3/2}$ and Ti $2p_{3/2}$ peaks. The figure also includes the results from curve fitting by two and one Voigt curves, respectively, keeping the peak positions, widths and shape factors fixed at the reported values for Cu, Cu^+ and Ti^{4+} with binding energies of E_b = 932.63, 932.18 and 485.46 eV, respectively [68]. The peak positions of these spectra indicate the presence of oxidized Cu^+ and Ti^{4+}, suggesting the formation of Cu_2O and TiO_2 on the Cu(001) surface, which is also confirmed by the corresponding O 1s peaks present at 530.20 and 529.70 eV (not shown) [68]. The overall oxide thickness d_{oxide} is estimated from the relative intensities of the Cu, Cu^+, and Ti^{4+} peaks. In particular, the intensity ratio I_{Cu+}/I_{Ti4+} indicates that the surface oxide contains 67±1 and 64±1 at.% TiO_2 for d_{Cu} = 9.90±0.05 and 14.70±0.05 nm, respectively, which is determined using the atomic sensitivity factors and assuming negligible electron absorption within the 1-2 nm thick oxide. The oxide thickness is then directly determined from the known thickness of the original Ti cap t_{Ti} = 4.0 ML, the measured TiO_2/Cu_2O atomic ratio, and the oxide densities of 4.23 and 6.00 g/cm^3, yielding d_{oxide} =1.76±0.05 and 1.89±0.05 nm for the two measured samples with d_{Cu} = 9.90 and 14.70 nm, respectively, indicating relatively good agreement between the two analyzed samples. Alternatively, d_{oxide} is determined using the intensity ratio $I_{Cu+}/I_{Cu,}$ [69]. For this analysis, the sample is approximated as a thick Cu layer covered with a uniformly mixed TiO_2/Cu_2O film with the above composition with the inelastic mean free path (IMFP) of 1.08±0.01 nm for Cu and a weighted electron inelastic mean free path (IMFP) of 1.31±0.01 nm for Cu^+ calculated using the NIST Electron IMFP Database (Version 1.2) software [70] which employs the predictive formula from Tanuma, Powell and Penn [71]. Applying this method to multiple spectra with different θ = 45-90° yields oxide thicknesses d_{oxide} = 1.96±0.09 and 1.71±0.09 nm for d_{Cu} = 9.90 and 14.70 nm, respectively, in good agreement (10% deviation) with d_{oxide} = 1.76±0.05 and 1.89±0.05 nm determined with the above method. We note here that this analysis assumes a uniform mixture of the oxide, which is an acceptable approximation for photoelectron emission at angles $\theta \geq 45°$ but not for small θ, for which the intensity ratio I_{Cu+}/I_{Ti4+} becomes a strong function of θ. This is shown in the main part of Figure 3(a), which is a plot of the angle resolved XPS Cu^+/Ti^{4+} peak intensity ratio as a function of the photoelectron emission angle θ relative to the surface, from the same two Cu layers with thickness d_{Cu} = 9.90

and 14.70 nm. As θ decreases from 90° to 45°, the measured I_{Cu+}/I_{Ti4+} increases slightly from 1.81 to 1.87 for d_{Cu} = 9.90 nm and from 2.16 to 2.40 for d_{Cu} = 14.70 nm. The reason for the 3-11% difference in the measured intensity ratio between the two samples is not known, as they have nominally the same Ti surface coverage, but may be related to slight experimental variations during the "uncontrolled" oxidation in laboratory air, which may also be the reason for the ~15% difference in d_{oxide}. Decreasing θ below 45° leads to a dramatic increase in the plotted ratio for both samples, reaching 5.57 and 14.55 at θ = 5°. At such an oblique angle, most XPS intensity originates from the top few monolayers. The fact that I_{Cu+} dominates over I_{Ti4+} for θ = 5° indicates that the top most surface layer consists of Cu_2O, while the Ti oxide is slightly below the surface, as quantified in more detail below.

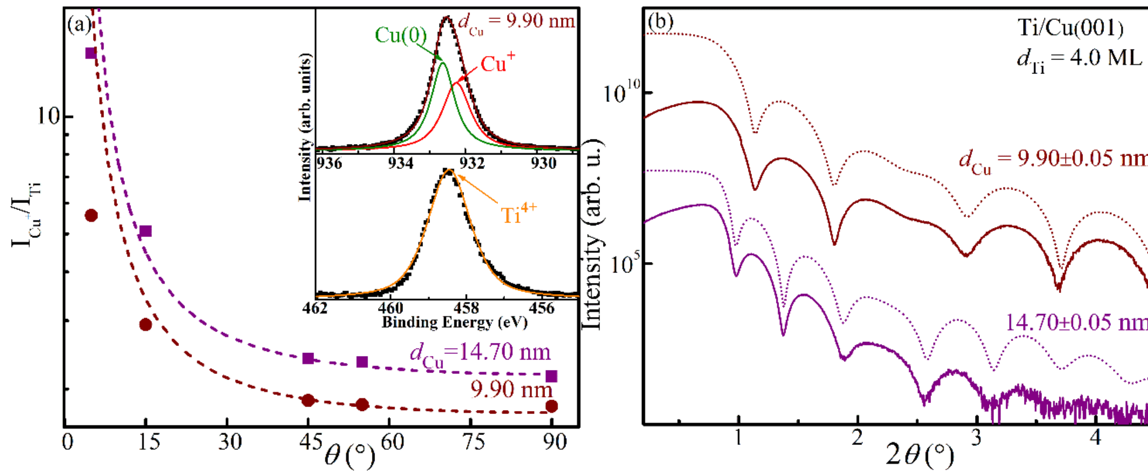

Figure 3. (a) The Cu^+-to-Ti^{4+} ratio of the XPS peak intensity I_{Cu+}/I_{Ti4+} vs photoelectron emission angle θ and (b) XRR θ-2θ spectra including the results from curve fitting (dotted lines), from 9.90 and 14.70 nm thick Cu(001) layers coated with 4.0 ML of Ti. The inset in (a) shows the Cu $2p_{3/2}$ and T_i $2p_{3/2}$ peaks measured at θ = 90°, including peak fitting.

Figure 3(b) shows typical θ-2θ XRR spectra for 2θ = 0.2-4.5°, which are used to determine the layer thickness and surface/interface roughness by fitting the spectra using the recursive theory of Parrat based on the Fresnel reflectivity formalism, assuming a Gaussian distribution to model the surface and interface roughness [72]. The resulting fitting curves are also plotted in Figure 3(b) as dotted lines which are shifted by two orders of magnitude for clarity purposes. The fitting procedure uses as a starting point, based on the XPS results above, a multilayer structure consisting of $Cu_2O/TiO_2/Cu$ with bulk densities of 6.0, 4.23 and 8.9 g/cm^3, respectively, on top of the MgO substrate. The oscillation period of the fringes provides values

for the thickness of the Cu layer as well as of each oxide layer: They are for the first sample d_{Cu} = 9.90±0.05 nm, d_{TiO2} = 1.39±0.05 nm, d_{Cu2O} = 0.46±0.03 nm, and for the second sample d_{Cu} = 14.70±0.05 nm, d_{TiO2} = 1.35±0.05 nm, d_{Cu2O} = 0.5±0.03nm. The sum of the two oxide thicknesses yield d_{oxide} = 1.85±0.06 nm for the two samples, in excellent agreement (5-6% deviation) from the XPS analysis above.

In a subsequent step of the XRR fitting procedure, the surface roughness and densities of TiO_2 or Cu_2O layers are adjusted such that the fitting curves match the measured doublet and bow shaped fringes at 2θ ranging between 1.8°-3° and 1.9°-2.6° on d_{Cu} = 9.90 and 14.70 nm, respectively. This approach is chosen because the shape and amplitude of the fringes are known to be primarily determined by the surface roughness and density variation of different layers [72]. Similarly complex fringe features at various different 2θ values are observed in the XRR spectra from all Cu films with d_{Cu} = 9-25 nm (not shown). The combined fitting from a set of 6 Ti-coated Cu(001) layers with different thickness results in a 11% correction of the TiO_2 density to 4.7±0.1 g/cm^3, while the Cu_2O density remains at the bulk value. It also provides values for the rms roughness of 0.90±0.10 nm for the Cu_2O surface and the Cu_2O-TiO_2 interface, and 0.60±0.02 and 0.70±0.02 nm for the TiO_2-Cu and Cu-MgO interfaces, respectively.

The fact that the measured density of the middle layer is larger than the TiO_2 bulk density indicates that it is not pure TiO_2 but contains 27±1 vol.% Cu_2O. To confirm this result, we calculate the expected angle resolved XPS intensity ratio I_{Cu+}/I_{Ti4+} for a two-layer oxide coating $Cu_2O/(TiO_2+Cu_2O)/Cu(001)$ by weighting atomic density and inelastic mean free paths for each layer, setting the ionization cross section ratio proportional to the elemental sensitivity factor ratio, and using the reported x-ray photoelectron intensity from multilayered native surface oxides [69]. The dashed lines in Figure 3(a) are the result of this analysis, using as a free fitting parameter the thickness d_1 of the Cu_2O surface layer, while the thickness d_2 of the mixed TiO_2+Cu_2O layer is constrained by the fixed total oxide thickness $d_{\mathrm{oxide}} = d_1 + d_2$. The curves fit the measured data reasonably well, with some deviation at small θ which is attributed to the larger effect from elastic electron scattering as reported from a study based on Monte Carlo simulations [73]. This fitting procedure yields d_1 = 0.40±0.01 nm and d_2 = 1.56±0.01 nm for d_{Cu} = 9.90 nm, and d_1 = 0.48±0.01 nm and d_2 = 1.23±0.01 nm for d_{Cu} = 14.70 nm. These values agree within 4-16% with the independent oxide thickness determination by XRR. In addition,

this XPS fitting indicates that the TiO_2+Cu_2O layer contains 27±1 and 24±1 vol% Cu_2O, in good agreement with the 27 vol.% Cu_2O obtained from the XRR analysis.

We attribute the presence of a Cu_2O surface layer as well as the TiO_2+Cu_2O alloy layer to intermixing of the Ti cap with the Cu layer prior to oxidation. Similar intermixing with Cu has been reported for various other transition metals including Fe [74], Co [57], Pd [75], and Ir [76], forming up to several monolayers thick alloy layers on top of a Cu surface, which has been attributed to the relief of misfit strain energy [77] and lowering the surface energy by forming alloys [57]. Particularly, the Cu surface energy γ = 1.8 J/m^2 (Ref. 78) is lower than that of Ti with γ = 2.1 J/m^2 (Ref. 78), providing a thermodynamic driving force for Cu segregation on top of the Ti surface, which may explain the Cu_2O surface oxide. The thermodynamic driving force remains even if considering the Cu-Ti interface energy of 0.1 J/m^2, as estimated from the free energy of mixing [79], or comparing the oxidized surface, since γ = 0.8 J/m^2 for Cu_2O (Ref. 80) is lower than γ = 1.2 J/m^2 for rutile TiO_2 (Ref. 81). A similar formation of Cu_2O surface oxides has been reported for the oxidation of TiCu and Ti_2Cu alloy films on Cu substrates, and has been attributed the considerably smaller activation energy for Cu diffusion in TiCu or Ti_2Cu than in Cu or that of Ti in TiCu or Ti_2Cu [82]. In summary, we conclude from the XPS and XRR analyses that during or after the room temperature Ti deposition, copper corresponding to a 0.45±0.05 nm thick layer diffuses into the 0.62±0.07 nm thick Ti cap layer, forming a CuTi alloy which, after air exposure, develops into a two layer Cu_2O/(TiO_2+Cu_2O) oxide with a total thickness of d_{oxide} = 1.83±0.09 nm.

Figure 4 shows the resistivity ρ vs. Cu thickness d_{Cu} = 9-25 nm, from epitaxial Cu(001) layers coated with 4 monolayers of Ti. The plot shows the measured ρ before and after air exposure at both 293 and 77 K, while the inset is from the pristine Cu(001) layers prior to the deposition of the Ti cap, as measured *in situ* at 293 K. The plot also shows as solid lines the predictions from the Fuchs-Sondheimer model [13,14], which are obtained by numerical integration of the formula from Ref. 83 that describes scattering at the two distinct top and bottom surfaces with the specularity parameters p_1 and p_2. Here, p_1 defines the specularity for electron scattering at the top surface, which corresponds to the Cu-vacuum interface for the pristine Cu samples, the Cu-Ti(Cu) interface for the Ti-coated layers, and the Cu-(TiO_2+Cu_2O) interface for the air-exposed samples. In our analysis, p_1 is the only fitting parameter while p_2 is kept constant, because the Cu-MgO interface is expected to be unaffected by the cap layer

deposition, air exposure, or Cu layer thickness d_{Cu}, and is set to $p_2 = 0$, based on the fact the Cu-MgO interface yields completely diffuse scattering according to our previous studies [27,28]. In addition, the Cu electron mean free path is set to the values from the free-electron model, $\lambda = 39$ and 313 nm at 293 and 77 K, respectively, and the bulk resistivity is set to the reported $\rho_o = 1.71$ μΩ-cm at 293 K and 0.213 μΩ-cm at 77 K.

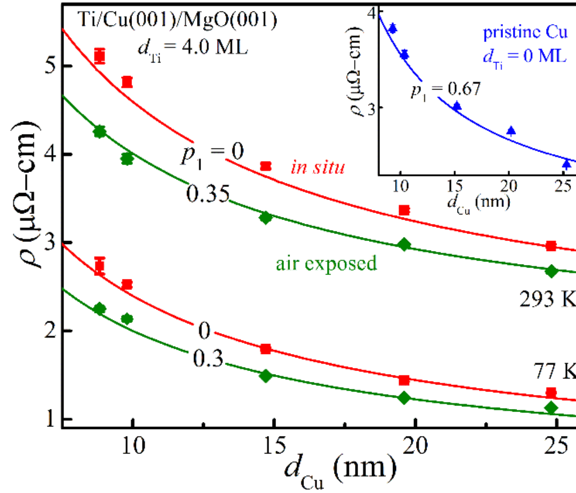

Figure 4. Resistivity ρ of epitaxial Cu(001) layers with a 4.0 ML of Ti cap vs thickness d_{Cu}, measured at 293 and 77 K before and after air exposure. The solid lines indicate predictions from the F-S model for surface specularity values p_1, as labeled, and the inset shows the corresponding resistivity prior to deposition of the Ti cap.

The resistivity of the pristine Cu layers plotted in the inset increases with decreasing d_{Cu} from 2.41±0.01 μΩ-cm for d_{Cu} = 25.3±0.1 nm to 3.82±0.04 μΩ-cm for d_{Cu} = 9.3±0.1 nm. This increase is caused by electron scattering at the top and bottom surfaces, that is, the Cu-vacuum and Cu-MgO interfaces. The data is best described by a specularity p_1 = 0.67±0.05, which is close to our previously reported p_1 = 0.7 for the Cu(001)-vacuum interface [27]**.** The resistivity of the Ti-coated layers measured in vacuum at 293 K increases from 2.96±0.02 μΩ-cm for d_{Cu} = 24.8±0.1 nm to 5.11±0.08 μΩ-cm for d_{Cu} = 8.8±0.1 nm, indicating a 23-34% larger resistivity in comparison to the corresponding pristine Cu layers. Fitting with the F-S model yields p_1 = 0±0.05 for the Ti-coated layers, suggesting that electron scattering at the Cu-Ti(Cu) interface is completely diffuse. This is also confirmed by the data for 77 K, which is well described with a p_1 = 0 curve. We note that the measured room temperature resistivity is 0.3% larger than the prediction for d = 24.8 nm, and this deviation increases with decreasing d to 3.6% for d = 8.8

nm. We attribute this deviation to the geometric effect of surface roughness which causes an additional increase in ρ with decreasing d [26], and also note that if initially assuming a $p_2 > 0$ would further increase this deviation. In addition, the data plotted for the Ti-coated layers includes a 0.45±0.05 nm correction to d_{Cu} since, as discussed and quantified above, Cu intermixing with the surface Ti causes a reduction in the effective Cu conducting thickness. Neglecting to account for this effect would increase the deviation of the measured resistivity and the $p_1 = 0$ curve by an additional 3.2-10.7%. After exposure to air for 30 minutes, ρ is reduced by 10-17% for d_{Cu} = 8.8-24.8 nm, which is consistent with the drop in R_s during the controlled oxidation experiment presented in Figure 1. Similarly, the resistivity measured at 77 K is 13-18% smaller after air exposure. Data fitting yields p_1 = 0.35±0.05 at 293 K, in good agreement with p_1 = 0.30±0.05 at 77 K, indicating partial specular scattering at the interface between Cu and TiO_2+Cu_2O.

The specular scattering at the pristine Cu surfaces is the consequence of the constructive interference of reflected electron plane waves from the relatively flat potential drop at the Cu-vacuum interface [27,29]. The subsequent decrease of p_1 from 0.67 to 0.0 during the addition of a Ti cap layer indicates a transition from partially specular to completely diffuse surface scattering, similar to what has been reported for 27-nm-thick Cu layers that have been coated with 1-4 monolayers of Ta [23] and consistent with first principle transport simulations indicating a comparable resistivity increase associated with Ti or Ta cap layers on Cu [30].

We attribute the completely diffuse scattering to (i) transitions of electrons near E_f between delocalized states in the Cu layer and localized Ti d-band states, effectively randomizing the electron momentum corresponding to diffuse surface scattering events which has been reported for Ni coated single crystal Cu [27], Co/Cu GMR structures [26,65] and Fe/Au (111) superlattices [36]**,** (ii) a lateral perturbation of the surface potential drop that diffusely scatters or terminates the electron plane wave at the crystal surface [85] due to Ti and Cu intermixing, and/or (iii) surface roughening which has been reported for Co/Cu GMR structures [86], Pt/Cu and Al/Cu bilayers [34] and Ni/Al trilayers [87].

During Ti oxidation, p_1 increases from 0 to 0.35±0.05, indicating a transition to partially specular scattering. This is attributed to a reduction in the LDOS at the Ti/Cu interface, with a calculated reduction in $N(E_f)$ by a factor of four (presented in Figure 2) that reduces the electron scattering probability into the localized states in the Ti cap layer. According to Ref. [40], the

interface reflection probability increases by nearly a factor of 3 when the LDOS is reduced by a factor of 2, resulting in electron channeling as reported for Fe/Au(100) superlattices [36,79]. Similarly, the conducting electron wave has a higher chance to be specularly reflected at the Cu-TiO_2+Cu_2O interface than at the Cu-Ti interface, resulting in a lower resistivity. A similar reduction of ρ during oxidation of a Co overlayer has been reported for Co/Cu spin valves, where a 1 Pa-s post-deposition O_2 exposure or a < 7×10^{-7} Pa O_2 partial pressure during the growth of Co monolayers on Cu increases the specular electron scattering [86]. It has been speculated that this effect is related to O_2 acting as surfactant for Co growth, or that the oxidation of protruding surface features effectively reduces the metal roughness [86]. However, a later study indicated that the interface scattering specularity remains unchanged if the interfacial roughness is reduced by a factor of six in Fe/Au multilayers [88], consistent with our interpretation stating that the primary reason for a resistivity decrease during Ti oxidation is associated with a reduction in the surface LDOS which confines the electron wave in the Cu layer and, in turn, increases the surface scattering specularity.

4. Conclusions

The sheet resistance R_s of Cu(001) layers increases with the addition of a Ti coating but decreases again upon O_2 exposure. This is attributed to changes in the specularity of the electron surface scattering. In particular, the scattering specularity at the Cu-vacuum interface is high, p = 0.67±0.05, which is attributed to constructive interference of the reflected electron plane waves from the relatively flat potential drop at the Cu-vacuum interface. In contrast, electron scattering at the Ti-coated Cu surface is completely diffuse, p = 0.00±0.05, which is attributed to localized states in Ti that cause a 4 times higher local density of states at the Fermi level than for the pristine Cu(001) surface. However, oxidation of the Ti cap results in partial recovery of the specular scattering, with p = 0.35±0.05 or 0.30±0.05 at 293 or 77 K, respectively, which is the result of a reduction of the local density of states at E_f by a factor of four during Ti oxidation. Combined XPS and XRR analyses indicate that oxygen exposure of a Cu surface that is coated with 4 ML of Ti results in the formation of a stack of Cu_2O/(TiO_2 +Cu_2O)/Cu(001), with a total oxide thickness of 1.83±0.09 nm. The overall results suggest that the specularity of electron surface scattering is primarily determined by the density of localized surface states at the Fermi level.

Supporting Information: (1) Data showing that polycrystalline Cu layers exhibit a similar increase and subsequent decrease in the resistance during deposition of a Ti cap and subsequent oxidation. (2) Atomic coordinates of the configurations corresponding to all the data points shown in Fig. 2(b). This material is available from IOP SST online.

Acknowledgements

The authors acknowledge support from the US National Science Foundation under grant No. 1309490, from the Semiconductor Research Corporation, under Tasks 1292.094 and 1292.078, and the STARnet FAME center funded by SRC, MARCO, and DARPA. Computational resources were provided by the Computational Center for Nanotechnology Innovations at RPI.

References

[1] Tao C, Cullen W G and Williams E D 2010 Visualizing the Electron Scattering Force in Nanostructures *Science (80-.).* **328** 736–40

[2] Liao L, Lin Y-C, Bao M, Cheng R, Bai J, Liu Y, Qu Y, Wang K L, Huang Y and Duan X 2010 High-speed graphene transistors with a self-aligned nanowire gate. *Nature* **467** 305–8

[3] Ahn Y, Jeong Y, Lee D and Lee Y 2015 Copper Nanowire-Graphene Core-Shell Nanostrucgure for Highly Stable Transparent Conducting Electrodes *ACS Nano* **9** 3125–33

[4] Chuang S, Gao Q, Kapadia R, Ford A C, Guo J and Javey A 2013 Ballistic InAs nanowire transistors *Nano Lett.* **13** 555–8

[5] Li A P, Clark K W, Zhang X G and Baddorf A P 2013 Electron transport at the nanometer-scale spatially revealed by four-probe scanning tunneling microscopy *Adv. Funct. Mater.* **23** 2509–24

[6] Lin H, Xu S, Wang X and Mei N 2013 Thermal and electrical conduction in ultrathin metallic films: 7 nm down to sub-nanometer thickness *Small* **9** 2585–94

[7] Mehta R, Chugh S and Chen Z 2015 Enhanced Electrical and Thermal Conduction in Graphene-Encapsulated Copper Nanowires *Nano Lett.* **15** 2024–30

[8] Maqableh M M, Huang X, Sung S-Y, Reddy K S M, Norby G, Victora R H and Stadler B J H 2012 Low-resistivity 10 nm diameter magnetic sensors. *Nano Lett.* **12** 4102–9

[9] Cheng Z, Liu L, Xu S, Lu M and Wang X 2015 Temperature Dependence of Electrical and Thermal Conduction in Single Silver Nanowire *Sci. Rep.* **5** 10718

[10] Kim T-H, Zhang X-G, Nicholson D M, Evans B M, Kulkarni N S, Radhakrishnan B, Kenik E a and Li A-P 2010 Large discrete resistance jump at grain boundary in copper nanowire. *Nano Lett.* **10** 3096–100

[11] Zhu Y F, Lang X Y, Zheng W T and Jiang Q 2010 Electron scattering and electrical conductance in polycrystalline metallic films and wires: Impact of grain boundary scattering related to melting point *ACS Nano* **4** 3781–8

[12] Xiang C, Güell A G, Brown M a., Kim J Y, Hemminger J C and Penner R M 2008 Coupled electrooxidation and electrical conduction in a single gold nanowire *Nano Lett.* **8** 3017–22

[13] Fuchs K 1938 The conductivity of thin metallic films according to the electron theory of metals *Math. Proc. Cambridge Philos. Soc.* **34** 100–8

[14] Sondheimer E H 1952 The mean free path of electrons in metals *Adv. Phys.* **1** 1–42

[15] Josell D, Brongersma S H and Tőkei Z 2009 Size-Dependent Resistivity in Nanoscale Interconnects *Annu. Rev. Mater. Res.* **39** 231–54

[16] Xu W, Wang L, Guo Z, Chen X, Liu J, Huang X, Matreials B F, Devices S, Machines I and Academy C 2015 Copper Nanowires as Nanoscale Interconnects : Their Stability , Electrical Transport , and Mechanical *ACS Nano* **9** 241–50

[17] Ye S, Rathmell A R, Chen Z, Stewart I E and Wiley B J 2014 Metal Nanowire Networks: The Next Generation of Transparent Conductors *Adv. Mater.* **26** 6670–87

[18] Eom H, Lee J, Pichitpajongkit A, Amjadi M, Jeong J-H, Lee E, Lee J-Y and Park I 2014 Ag@Ni Core-Shell Nanowire Network for Robust Transparent Electrodes Against Oxidation and Sulfurization. *Small* **10** 4171–81

[19] Rathmell A R, Nguyen M, Chi M and Wiley B J 2012 Synthesis of oxidation-resistant cupronickel nanowires for transparent conducting nanowire networks. *Nano Lett.* **12** 3193–9

[20] Boukai A, Xu K and Heath J R 2006 Size-dependent transport and thermoelectric properties of individual polycrystalline bismuth nanowires *Adv. Mater.* **18** 864–9

[21] Zuev Y M, Lee J S, Galloy C, Park H and Kim P 2010 Diameter dependence of the transport properties of antimony telluride nanowires *Nano Lett.* **10** 3037–40

[22] Rakheja S, Chang S C and Naeemi A 2013 Impact of dimensional scaling and size effects on spin transport in copper and aluminum interconnects *IEEE Trans. Electron Devices* **60** 3913–9

[23] Chawla J S and Gall D 2009 Specular electron scattering at single-crystal Cu(001) surfaces *Appl. Phys. Lett.* **94** 252101

[24] Chawla J S, Zahid F, Guo H and Gall D 2010 Effect of O[sub 2] adsorption on electron scattering at Cu(001) surfaces *Appl. Phys. Lett.* **97** 132106

[25] Timalsina Y P, Shen X, Boruchowitz G, Fu Z, Qian G, Yamaguchi M, Wang G-C, Lewis K M and Lu T-M 2013 Evidence of enhanced electron-phonon coupling in ultrathin epitaxial copper films *Appl. Phys. Lett.* **103** 191602

[26] Timalsina Y P, Horning A, Spivey R F, Lewis K M, Kuan T-S, Wang G-C and Lu T-M 2015 Effects of nanoscale surface roughness on the resistivity of ultrathin epitaxial copper films *Nanotechnology* **26** 075704

[27] Zheng P Y, Deng R P and Gall D 2014 Ni doping on Cu surfaces: Reduced copper resistivity *Appl. Phys. Lett.* **105** 131603

[28] Chawla J S, Zhang X Y and Gall D 2011 Epitaxial TiN(001) wetting layer for growth of thin single-crystal Cu(001) *J. Appl. Phys.* **110** 043714

[29] Ke Y, Zahid F, Timoshevskii V, Xia K, Gall D and Guo H 2009 Resistivity of thin Cu films with surface roughness *Phys. Rev. B* **79** 155406

[30] Zahid F, Ke Y, Gall D and Guo H 2010 Resistivity of thin Cu films coated with Ta, Ti, Ru, Al, and Pd barrier layers from first principles *Phys. Rev. B* **81** 045406

[31] Yokogawa S and Kakuhara Y 2011 Role of Impurity Segregation into Cu/Cap Interface and Grain Boundary in Resistivity and Electromigration of Cu/Low- k Interconnects *Jpn. J. Appl. Phys.* **50** 05EA02

[32] Shimada M, Moriyama M, Ito K, Tsukimoto S and Murakami M 2006 Electrical resistivity of polycrystalline Cu interconnects with nano-scale linewidth *J. Vac. Sci. Technol. B Microelectron. Nanom. Struct.* **24** 190

[33] Sun T, Yao B, Warren A, Barmak K, Toney M, Peale R and Coffey K 2009 Dominant role of grain boundary scattering in the resistivity of nanometric Cu films *Phys. Rev. B* **79**

041402

[34] Rossnagel S M and Kuan T S 2004 Alteration of Cu conductivity in the size effect regime *J. Vac. Sci. Technol. B Microelectron. Nanom. Struct.* **22** 240

[35] Butler W, Zhang X-G, Nicholson D, Schulthess T and MacLaren J 1996 Giant Magnetoresistance from an Electron Waveguide Effect in Cobalt-Copper Multilayers *Phys. Rev. Lett.* **76** 3216–9

[36] Dekadjevi D, Ryan P, Hickey B, Fulthorpe B and Tanner B 2001 Experimental Evidence for Electron Channeling in Fe /Au (100) Superlattices *Phys. Rev. Lett.* **86** 5787–90

[37] Vedyayev A, Cowache C, Ryzhanova N and Dieny B 1999 Quantum effects in the giant magnetoresistance of magnetic multilayered structures *J. Phys. Condens. Matter* **5** 8289–304

[38] Stiles M D 1996 Giant Magnetoresistance and Magnetic Multilayers Jeff Childress , Chairman Spin-dependent interface transmission and reflection in magnetic multilayers (invited) *J. Appl. Phys.* **79** 5805

[39] Hood R Q and Falicov L M 1992 Boltzmann-equation approach to the negative magnetroresistance of ferromatic-normal metal multilayers *Phys. Rev. B* **46** 8287

[40] Chico L and Falicov L M 1995 Electron scattering at interfaces: A tight-binding approach *Phys. Rev. B* **52** 6640

[41] Bailey W E, Fery C, Yamada K and Wang S X 1999 Direct measurement of surface scattering in giant magnetoresistance spin valves *J. Appl. Phys.* **85** 7345

[42] Tsymbal E and Pettifor D 1996 Effects of band structure and spin-independent disorder on conductivity and giant magnetoresistance in Co/Cu and Fe/Cr multilayers *Phys. Rev. B* **54** 15314–29

[43] Ito K, Tsukimoto S, Kabe T, Tada K and Murakami M 2007 Effects of Substrate Materials on Self-Formation of Ti-Rich Interface Layers in Cu(Ti) Alloy Films *J. Electron. Mater.* **36** 606–13

[44] Kohama K, Ito K, Mori K, Maekawa K, Shirai Y and Murakami M 2009 Rutherford Backscattering Spectrometry Analysis of Self-Formed Ti-Rich Interface Layer Growth in Cu(Ti)/Low-k Samples *J. Electron. Mater.* **38** 1913–20

[45] Sakata A, Kato S, Yano Y, Toyoda H, Kawanoue T, Hatano M, Wada J, Yamada N, Oki T, Yamaguchi H, Nakamura N, Higashi K, Yamada M, Fujimaki T and Hasunuma M 2008 Copper Line Resistance Control and Reliability Improvement by Surface Nitridation of Ti barrier Metal *2008 Int. Interconnect Technol. Conf.* 165–7

[46] Kitada H, Suzuki T, Akiyama S and Nakamura T 2009 Influence of Titanium Liner on Resistivity of Copper Interconnects *Jpn. J. Appl. Phys.* **48** 04C026

[47] César M, Liu D, Gall D and Guo H 2014 Calculated Resistances of Single Grain Boundaries in Copper *Phys. Rev. Appl.* **2** 044007

[48] Henriquez R, Moraga L, Kremer G, Flores M, Espinosa A and Munoz R C 2013 Size effects in thin gold films: Discrimination between electron-surface and electron-grain boundary scattering by measuring the Hall effect at 4 K *Appl. Phys. Lett.* **102** 4–8

[49] Purswani J M and Gall D 2008 Surface morphological evolution during annealing of

epitaxial Cu(001) layers *J. Appl. Phys.* **104** 044305

[50] Cazottes S, Zhang Z L, Daniel R, Chawla J S, Gall D and Dehm G 2010 Structural characterization of a Cu/MgO(001) interface using CS-corrected HRTEM *Thin Solid Films* **519** 1662–7

[51] Deng R, Ozsdolay B D, Zheng P Y, Khare S V. and Gall D 2015 Optical and transport measurement and first-principles determination of the ScN band gap *Phys. Rev. B* **91** 045104

[52] Deng R, Zheng P and Gall D 2015 Epitaxial Sc 1À x Ti x N „ 001: Optical and electronic transport properties *J. Appl. Phys.* **118** 015706

[53] Zheng P, Ozsdolay B D and Gall D 2015 Epitaxial growth of tungsten layers on MgO (001) *J. Vac. Sci. Technol. A Vacuum, Surfaces, Film.* **33** 061505–1 – 7

[54] Blöchl P E 1994 Projector augmented-wave method *Phys. Rev. B* **50** 17953–79

[55] Kresse G 1999 From ultrasoft pseudopotentials to the projector augmented-wave method *Phys. Rev. B* **59** 1758–75

[56] Perdew J, Burke K and Ernzerhof M 1996 Generalized Gradient Approximation Made Simple. *Phys. Rev. Lett.* **77** 3865–8

[57] Fassbender J, Allenspach R and Dürig U 1997 Intermixing and growth kinetics of the first Co monolayers on Cu(001) *Surf. Sci.* **383** L742–8

[58] Schneider C M, Bressler P, Schuster P, Kirschner J, De Miguel J J and Miranda R 1990 Curie temperature of ultrathin films of fcc-cobalt epitaxially grown on atomically flat Cu(100) surfaces *Phys. Rev. Lett.* **64** 1059–62

[59] Kado T 2000 Structure of Ti films deposited on MgO(001) substrates *Surf. Sci.* **454** 783–9

[60] Press W H, Teukolsky S A, Vetterling W T and Flannery B P 1992 *Numerical Recipes in C: The Art of Scientific Computing* Cambridge University Press; Cambridge

[61] Zhou G and Yang J C 2011 Initial Oxidation Kinetics of Cu(100), (110), and (111) Thin Films Investigated by in Situ Ultra-high-vacuum Transmission Electron Microscopy *J. Mater. Res.* **20** 1684–94

[62] Revie R Wi and H.Herbert U 2008 *Corrosion and Corrosion Control: An introduction to corrosion science and engineering* John Wiley & Sons, Inc., New Jersey, p.224-247.

[63] Uhlig H H 1956 Initial oxidation rate of metals and the logarithmic equation *Acta Metall.* **4** 541–54

[64] Smith J R, Gay J G and Arlinghas F J 1980 Self consistent local-orbital method for calculating surface electronic structure : Applicaiton to Cu (100) *Phys. Rev. B* **21** 2201–21

[65] Burdick G a. 1963 Energy band structure of copper *Phys. Rev.* **129** 138–50

[66] Landmann M, Rauls E and Schmidt W G 2012 The electronic structure and optical response of rutile, anatase and brookite TiO2. *J. Phys. Condens. Matter* **24** 195503

[67] Oshikiri M, Boero M, Ye J, Aryasetiawan F and Kido G 2003 The electronic structures of the thin films of InVO4 and TiO2 by first principles calculations *Thin Solid Films* **445** 168–74

[68] Biesinger M C, Lau L W M, Gerson A R and Smart R S C 2010 Resolving surface chemical states in XPS analysis of first row transition metals, oxides and hydroxides: Sc, Ti, V, Cu and Zn *Appl. Surf. Sci.* **257** 887–98

[69] Mccafferty E and Wightman J P 1998 Determination of the Concentration of Surface Hydroxyl Groups on Metal Oxide Films by a Quantitative XPS Method *Surf. Interface Anal.* **26** 549–64

[70] C. J. Powell, A. Jablonski, NIST Electron Inelastic-Mean-Free-Path Database - Version 1.2

[71] Tanuma S, Powell C J and Penn D R 1991 Calculations of electorn inelastic mean free paths. II. Data for 27 elements over the 50-2000 eV range *Surf. Interface Anal.* **17** 911–26

[72] Parratt L G 1954 Surface Studies of Solids *Phys. Rev. Lett.* **95** 359–69

[73] Baschenko O A and Nefedov V I 1982 Relative intensities in x-ray photoelectron spectra. part ix. estimates for photoelectron mean free paths taring into account elastic collisions in a solid* *J. Electron Spectros. Relat. Phenomena* **27** 109–18

[74] Meyerheim H L, Popescu R, Sander D, Kirschner J, Robach O and Ferrer S 2005 Layer relaxation and intermixing in Fe/Cu(001) studied by surface x-ray diffraction *Phys. Rev. B - Condens. Matter Mater. Phys.* **71** 035409

[75] Murray P W, Stensgaard I, Lægsgaard E and Besenbacher F 1995 Mechanisms of initial alloy formation for Pd on Cu(100) studied by STM *Phys. Rev. B* **52** R14 404

[76] Gilarowski G and Niehus H 1999 Intermixing and subsurface alloy formation: Ir on Cu(100) *Surf. Sci.* **436** 107–20

[77] Tersoff J 1982 Surface Confined alloy foramiton in immiscible systems *Phys. Rev. Lett.* **48** 434–7

[78] Vitos L, Ruban A V, Skriver H L and Kolla J 1998 The surface energy of metals *Surf. Sci.* **411** 186–202

[79] Battezzati L, Baricco M, Riontino G and Soletta I 1990 THERMODYNAMIC EVALUATION OF THE Cu-Ti SYSTEM IN VIEW OF SOLID STATE AMORPHIZATION REACTIONS To cite this version : *J. Phys. Colloq.* **51** C4–79 – C4–85

[80] Zhou G, Fong D, Wang L, Fuoss P, Baldo P, Thompson L and Eastman J 2009 Nanoscale duplex oxide growth during early stages of oxidation of Cu-Ni(100) *Phys. Rev. B* **80** 134106

[81] Perron H, Domain C, Roques J, Drot R, Simoni E and Catalette H 2007 Optimisation of accurate rutile TiO2 (110), (100), (101) and (001) surface models from periodic DFT calculations *Theor. Chem. Acc.* **117** 565–74

[82] Bateni M R, Mirdamadi S, Ashrafizadeh F, Szpunar J a. and Drew R a L 2001 Oxidation behaviour of titanium coated copper substrate *Surf. Coatings Technol.* **139** 192–9

[83] Chawla J S, Gstrein F, O'Brien K P, Clarke J S and Gall D 2011 Electron scattering at surfaces and grain boundaries in Cu thin films and wires *Phys. Rev. B* **84** 235423

[84] Bailey W, Wang S and Tsymbal E 2000 Electronic scattering from Co/Cu interfaces: In situ measurement and comparison with theory *Phys. Rev. B* **61** 1330–5

[85] Greene R and O'Donnell R 1966 Scattering of Conduction Electrons by Localized Surface Charges *Phys. Rev. Lett.* **147** 599

[86] Egelhoff W F, Chen P J, Powell C J, Stiles M D and Mcmichael R D 1997 Oxygen as a surfactant in the growth of giant magnetoresistance spin valves *J. Appl. Phys.* **82** 6142

[87] Aurongzeb D, Holtz M, Berg J M, Chandolu a. and Temkin H 2005 The influence of interface roughness on electrical transport in nanoscale metallic multilayers *J. Appl. Phys.* **98** 063708

[88] Cole A, Hickey B J, Hase T P a, Buchanan J D R and Tanner B K 2004 Influence of the interfacial roughness on electron channelling in Fe/Au(001) multilayers *J. Phys. Condens. Matter* **16** 1197–209